

GRAVITATIONAL LENSING MAGNIFICATION AND TIME DELAY STATISTICS FOR DISTANT SUPERNOVAE

MASAMUNE OGURI,¹ YASUSHI SUTO,^{1,2} AND EDWIN L. TURNER³
 oguri@utap.phys.s.u-tokyo.ac.jp, suto@phys.s.u-tokyo.ac.jp, elt@astro.princeton.edu

RESCEU-13/02 UTAP-420

ABSTRACT

Strong gravitational lensing of distant supernovae (SNe), particularly Type Ia's, has some exploitable properties not available when other sorts of cosmologically distant sources are lensed. One such property is that the "standard candle" nature of SN at peak brightness allows a direct determination of the lensing magnification factor for each well observed image. Another is that the duration of a SN event is of the same order as the differential time delays between the various lens images for roughly galaxy mass lensing objects. A relatively precise constraint on each image's magnification leads to better constraints on the lens mass model than are available in more familiar lens systems, and the comparable time scales of the photometric event and the time delay invite a variety of applications, including high precision measurements of the delay and the targeting of especially interesting phases of the explosion (including its very early stages) for intensive observation when they appear in trailing images.

As an initial exploration of these possibilities we present calculations of SN lensing statistics in a "concordance cosmology" assuming a simple spherical model for lens mass distributions. We emphasize magnification and time delay effects. Plausible SN surveys, such as the proposed *SNAP* space mission, would discover several to some tens of strongly lensed SNe Ia per year, and at least a few of these will be at redshifts well beyond those that would be accessible via unlensed events. The total number of such anomalously high redshift SNe Ia will be a useful test of high redshift star formation models. SN surveys of finite duration will, of course, miss the appearance of some images, and the effect becomes large when the delay approaches the survey duration; we quantify this selection bias. Finally, we investigate how well the appearance of trailing images can be predicted based on various amounts of available information on the lensing event. Knowledge of the magnification factor for the leading (and brighter) image makes it possible to predict the appearance of a trailing image relatively accurately if the lens redshift is also known.

Subject headings: cosmology: theory — gravitational lensing — supernovae: general

1. INTRODUCTION

Recent systematic surveys of distant type Ia supernovae (hereafter SNe Ia) strongly suggest the presence of *dark energy* which may dominate the total energy density of the universe (Riess et al. 1998; Perlmutter et al. 1999). The reason that this rather surprising conclusion is taken so seriously stems from the fact that the SNe Ia are excellent (albeit empirical) "standard candle" distance indicators, after an appropriate correction for the peak luminosity dependence on the shape of the individual lightcurve (Phillips 1993; Riess, Press, & Kirshner 1996). The exploitation of SNe Ia as cosmological probes has already been extensive (Riess et al. 1998; Perlmutter et al. 1999), and plans for yet more extensive observational studies, such as *LSST*⁴ (Large-aperture Synoptic Survey Telescope), are being rapidly developed. The most ambitious of these is the proposed satellite *SNAP*⁵ (SuperNova/Acceleration Probe) which would gather ~ 2000 SNe Ia per year by frequently imaging ~ 20 square degrees of sky.

In this paper we explore some other ways in which the unique transient "standard candle" properties of SNe Ia might be exploited for those few which happen to be strongly gravitation-

ally lensed by an intervening object of roughly galactic mass. For the sake of specificity we will adopt the observational parameters associated with the proposed *SNAP* mission unless otherwise stated.

Very roughly 0.1 percent of sources at $z > 1$ are expected to have multiple images due to strong gravitational lensing (e.g., Turner, Ostriker, & Gott 1984), and *SNAP* therefore would find at least ~ 2 lensed SNe Ia per year (e.g., Holz 2001). They will be qualitatively different from the lensed systems so far detected (e.g., ~ 60 QSO multiple-image systems⁶). First of all, the time-delay between the multiple images could be robustly and accurately determined for each object, at least in principle. Indeed, for a typical cosmological lensing time delay, of an order of a year, it is unlikely that one will observe all of the multiple images *simultaneously* due to the finite duration of SNe Ia (\sim a month). This also means that some lensing events may be missed because the observation time is finite; one or more multiple images may appear only before or after the observing season or program. This is in marked contrast to QSO multiple-image systems where the images are observed simultaneously and their presence and geometrical arrangement in the sky is often the chief indication of lensing. Furthermore, since the SNe

¹ Department of Physics, School of Science, University of Tokyo, Tokyo 113-0033, Japan

² Research Center for the Early Universe (RESCEU), School of Science, University of Tokyo, Tokyo 113-0033, Japan

³ Princeton University Observatory, Peyton Hall, Princeton, NJ 08544

⁴ <http://www.lsst.org/lsst/>

⁵ <http://snap.lbl.gov/>

⁶ A summary of known lensed QSO systems is available on the CASTLES homepage (Kochanek, C. S., Falco, E. E., Impey, C., Lehar, J., McLeod, B., & Rix, H.-W., <http://cfa-www.harvard.edu/castles/>)

Ia are believed to be a reliable “standard candle”, the magnification factor of the lensing can be determined directly. This is not feasible for any other sources because an object’s intrinsic luminosity is basically unknown. This can provide valuable additional information on the lensing potential. With such information, one may indeed *predict* the location and the epoch of the additional trailing images, at least statistically.

In the present paper, we first analytically calculate the expected number of lensed SNe Ia to be found by a *SNAP*-like survey, including the effects of time delay bias due to a finite observation/survey duration. Since lens systems with wider separations have larger time delays on average, time delay bias becomes more significant for bigger image separations. Next we describe ways to predict the appearance of additional images of lensed SNe Ia. We then briefly consider the consequences of using a different and perhaps more realistic model for lens mass distributions. In conclusion, we discuss some of the implications and possible extensions of this work.

Since we are not here concerned with determining cosmological parameters via lensing (although this constitutes one of the primary purposes of the SNe Ia survey), unless otherwise specified we simply adopt the lambda-dominated universe with $(\Omega_0, \lambda_0, h) = (0.3, 0.7, 0.7)$, where Ω_0 is the density parameter, λ_0 is the cosmological constant, h is the Hubble constant in units of $100 \text{ km s}^{-1} \text{ Mpc}^{-1}$, the so called concordance cosmology (Ostriker & Steinhardt 1995; Bahcall et al. 1999).

2. NUMBER COUNTS OF SUPERNOVA IA

The number of SNe is closely related to the star formation rate R_{SF} in the universe. For a Salpeter initial mass function ($\phi_{\text{IMF}}(M) \propto M^{-2.35}$, $0.1M_{\odot} < M < 125M_{\odot}$), the rate of Type Ia events R_{SNeIa} is calculated as follows (Madau, Della Valle, & Panagia 1998)

$$R_{\text{SNeIa}}(z) = \frac{\eta \int_0^{t(z)} R_{\text{SF}}(z(t')) dt' \int_{M_c}^{8M_{\odot}} \exp[-(t-t'-t_M)/\tau] \phi_{\text{IMF}}(M) dM}{\tau \int M \phi_{\text{IMF}}(M) dM} \quad (1)$$

where $M_c = \max[3M_{\odot}, (10 \text{ Gyr}/t')^{0.4} M_{\odot}]$ is the minimum mass of a star that reaches the white dwarf phase at time t' (assuming all systems with the primary star of mass $3M_{\odot} \leq M \leq 8M_{\odot}$ are possible progenitors of SNe Ia), $t_M = 10 \text{ Gyr}/(M[M_{\odot}])^{2.5}$ is the standard lifetime of a star of mass M , τ is a characteristic explosion time scale (corresponding to an effective “delay” time scale after the collapse of the primary star to a white dwarf), η is the SNe Ia explosion efficiency. We adopt three representative star formation rates used by Porciani & Madau (2001). The explicit forms of these in an Einstein-de Sitter universe are

$$R_{\text{SF1}}(z) = 0.462h \frac{\exp(3.4z)}{\exp(3.8z)+45} M_{\odot} \text{ yr}^{-1} \text{ Mpc}^{-3}, \quad (2)$$

$$R_{\text{SF2}}(z) = 0.230h \frac{\exp(3.4z)}{\exp(3.4z)+22} M_{\odot} \text{ yr}^{-1} \text{ Mpc}^{-3}, \quad (3)$$

$$R_{\text{SF3}}(z) = 0.308h \frac{\exp(3.05z-0.4)}{\exp(2.93z)+15} M_{\odot} \text{ yr}^{-1} \text{ Mpc}^{-3}. \quad (4)$$

The first model (SF1) includes a correction for dust reddening, and matches most measured UV-continuum and H α luminosity densities (Madau & Pozzetti 2000). The second model (SF2) is also possible because of the uncertainties associated with the incompleteness of data sets and the amount of dust

extinction (Steidel et al. 1999). The third model (SF3) is considered because it has been suggested that the rates at high z may have been severely underestimated due to an unexpectedly large amount of dust extinction (e.g., Blain et al. 1999). These star formation rates are easily converted to those in different cosmologies (Porciani & Madau 2001), and are considered to span the range of reasonably realistic possibilities.

The number rate of SNe Ia which occur between z and $z+dz$ is then

$$\frac{dN}{dz} = \frac{R_{\text{SNeIa}}(z)}{1+z} \frac{\Omega_A D_A^2(z)}{H(z)(1+z)} (1+z)^3, \quad (5)$$

where Ω_A is the solid angle of the observed region and $D_A(z)$ is the angular diameter distance.

3. LENSING STATISTICS

3.1. Image Separation and Time Delay Probability Distribution

In this discussion, we omit the magnification bias (Turner 1980; Turner et al. 1984) because the intrinsic luminosity function at peak brightness of Type Ia SNe is quite narrow⁷. We consider that magnification of SNe at redshifts beyond those normally accessible to the survey, another form of magnification bias, separately in the next subsection.

We now consider lensing objects with a the Singular Isothermal Sphere (SIS) density profile:

$$\rho(r) = \frac{v^2}{2\pi G r^2}, \quad (6)$$

where v is a one-dimensional velocity dispersion and define the characteristic scale length

$$\xi_0 = 4\pi \left(\frac{v}{c}\right)^2 \frac{D_{\text{OL}} D_{\text{LS}}}{D_{\text{OS}}}, \quad (7)$$

where D_{OL} , D_{OS} , and D_{LS} are the angular diameter distances to the lens, to the source, and between the lens and source, respectively. Then the lens equation becomes $y = x - x/|x|$, where x and y are image and source positions in each plane normalized by ξ_0 and $\xi_0 D_{\text{OS}}/D_{\text{OL}}$, respectively. This has two solutions $x_{\pm} = y \pm 1$, and each image will be magnified by a factor $\mu_{\pm} = (1/y) \pm 1$. The angular separation of two images is given by

$$\theta = \frac{\xi_0(x_+ - x_-)}{D_{\text{OL}}} = 8\pi \left(\frac{v}{c}\right)^2 \frac{D_{\text{LS}}}{D_{\text{OS}}}. \quad (8)$$

The differential time delay between two images can also be calculated as

$$c\Delta t(y) = 32\pi^2 \left(\frac{v}{c}\right)^4 \frac{D_{\text{OL}} D_{\text{LS}}}{D_{\text{OS}}} (1+z_{\text{L}}) y. \quad (9)$$

The cumulative and differential probability distributions of strong lensing are

$$P(>\theta; z_{\text{S}}) = \int_0^{z_{\text{S}}} dz_{\text{L}} \int_{v_{\text{min}}}^{\infty} \sigma_{\text{SIS}} \frac{c dt}{dz_{\text{L}}} (1+z_{\text{L}})^3 \phi(v), \quad (10)$$

$$P(\theta; z_{\text{S}}) = -\frac{d}{d\theta} P(>\theta; z_{\text{S}}), \quad (11)$$

where $\sigma_{\text{SIS}} = \pi \xi_0^2$ is the cross section of strong lensing, $v_{\text{min}} = (\theta/8\pi)^{1/2} (D_{\text{OS}}/D_{\text{LS}})^{1/2} c$, and $\phi(v)$ is the velocity function of lens galaxies. We adopt the velocity function:

$$\phi(v) dv = \frac{\Psi_*}{\ln 10} \left(\frac{\sqrt{2}v}{v_*}\right)^{\beta} \exp\left[-\left(\frac{\sqrt{2}v}{v_*}\right)^{\beta/2.5}\right] \frac{dv}{v_*}, \quad (12)$$

⁷ This is equivalent to assuming that the survey monitors every field sufficiently frequently to catch each SN event near its peak brightness, as is the case for *SNAP*. The bias could not be neglected for a more traditional survey which finds most objects well after their maximum brightness.

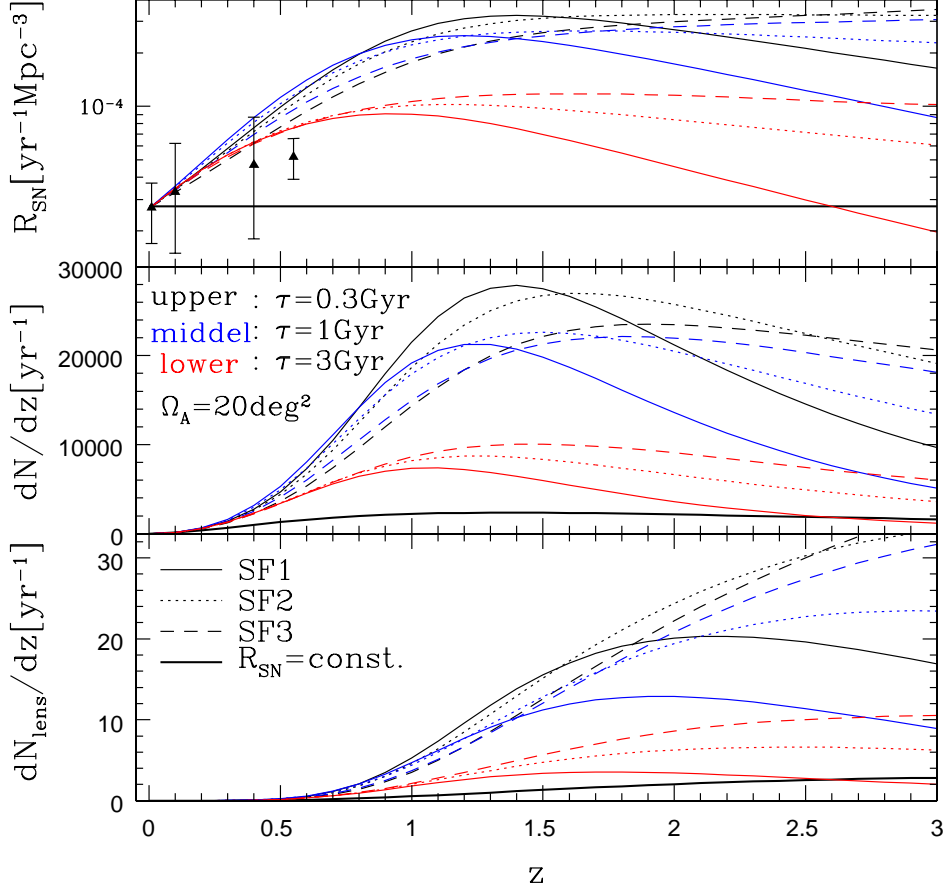


FIG. 1.— Supernova rates R_{SN} (eq. [1]), number rates of SNe Ia dN/dz (eq. [5]), and number rates of lensed SNe Ia $dN_{\text{lens}}/dz = \int dN/dz P(z) dz$ as a function of redshift of SNe Ia, on the basis of the model described in §2. In the middle and bottom panels, observations of 20 square degrees field is assumed and no magnitude limit is imposed. For R_{SN} , four observed SN Ia rates are also plotted by filled triangles; $z \sim 0.01$ (Cappellaro, Evans, & Turatto 1999), $z \sim 0.1$ (Hardin et al. 2000), $z \sim 0.4$ (Pain et al. 1996), and $z \sim 0.55$ (Pain et al. 2002). The efficiency parameter η is adjusted so as to reproduce the observed SN Ia rate at $z \sim 0.01$. The “concordance” lambda-dominated universe with $(\Omega_0, \lambda_0, h) = (0.3, 0.7, 0.7)$ is assumed.

where $\Psi_* = 7.3 \times 10^{-2} h^3 \text{Mpc}^{-3}$, $\beta = -1.3$, and $v_* = 247 \text{km s}^{-1}$. This distribution function is based on the Southern Sky Redshift Survey and is derived by Gonzalez et al. (2000). Averaging the above probability function for fixed z_S over the observed rate of SNe (eq. [5]) yields the number rate of strong lensing:

$$P(\theta) = \int P(\theta; z_S) \frac{dN}{dz_S} dz_S. \quad (13)$$

Similarly, the joint probability distributions of time delays and image separations are (see eqs. [29]-[31] of Oguri et al. 2002)

$$P(> \Delta t, \theta; z_S) = \int_0^{z_S} dz_L \left[\frac{dv}{d\theta} \sigma_{\text{SIS}} N^T(> \Delta t) \frac{cdt}{dz_L} (1+z_L)^3 \phi(v) \right]_{v=v_{\min}} \quad (14)$$

$$P(\Delta t, \theta; z_S) = -\frac{d}{d(\Delta t)} P(> \Delta t, \theta; z_S), \quad (15)$$

where $N^T(> \Delta t) = 1 - y_{\min}^2$ and y_{\min} can be calculated from $\Delta t = \Delta t(y_{\min})$. These joint probability distributions divided by $P(\theta; z_S)$ give the conditional probability distributions $P(> \Delta t | \theta; z_S)$ and $P(\Delta t | \theta; z_S)$.

Figure 1 shows the predicted number rates of SNe Ia and also the expected number rate of lensed SNe Ia. The number rates of SNe Ia are calculated from equation (5). It is clear from this figure that the number of SNe Ia strongly depends on the

star formation rate and its evolution, as indicated by Madau et al. (1998). The number of lensed SNe Ia also shows large differences between models, reflecting the above sensitive model-dependence of the number of SNe Ia. Our calculation predicts that the number of strongly lensed SNe Ia will be between a few and a few tens per year for a *SNAP*-like survey. These lensing rates are roughly consistent with those calculated by Wang (2000) and Holz (2001).

3.2. SNe beyond the Magnitude Limit

Gravitational lensing magnifies SNe, thus some SNe which exceed the magnitude limit if they are unlensed might be observed due to their magnification (e.g., Kolatt & Bartelmann 1998; Porciani & Madau 2000; Sullivan et al. 2000; Goobar et al. 2002). If we neglect the effect of gravitational lensing, the apparent magnitude of SNe at peak can be expressed as

$$m_X = M_B + 5 \log(D_L(z)[\text{Mpc}]) + 25 + K_{BX}, \quad (16)$$

where $M_B = -19.4$ is the peak magnitude of SNe Ia, $D_L(z) = (1+z)^2 D_A(z)$ is luminosity distance, and K_{BX} is the single- or cross-filter K-corrections. Therefore, even for high- z SNe Ia whose unlensed apparent magnitude exceeds the magnitude limit, $m_X > m_{\text{lim}}$, they are observed if magnified by a factor μ satisfying

$$\mu \geq 10^{0.4(m_X - m_{\text{lim}})} \equiv \mu_{\min}. \quad (17)$$

We consider the following two cases: (1) $\mu_{\text{--}} > \mu_{\min}$. This corresponds to the case that both lensed images are observed. (2)

$\mu_+ > \mu_{\min}$. This means that at least one image is observed. In each case, the cross section for lensing is

$$\sigma(\mu_{\mp} > \mu_{\min}) = \frac{\sigma_{\text{SIS}}}{(\mu_{\min} \pm 1)^2}. \quad (18)$$

We calculate the numbers of such lensed SNe Ia, and the results are shown in Figure 2. We assume the magnitude limit is $m_{\text{lim}} = 30$, and also impose a requirement that the photometry must extend to 3.8 magnitudes below peak. We take account of the intrinsic dispersion of SNe Ia peak magnitudes assuming the Gaussian distribution with dispersion $\sigma_m = 0.15$ (Porciani & Madau 2000). As seen in the figure, the expected number of such lensed SNe Ia depends very strongly on models of star formation history. In most models, however, more than one high- z ($z \sim 3$) SNe Ia per year is expected to be observed. Actually the difference simply comes from the difference in supernova rates, thus we can infer supernova rates at high redshifts from the observed number of lensed SNe Ia. The supernova rate as a function of redshift is useful not only to constrain progenitor models and star formation history (e.g., Yungelson & Livio 2000) as shown in these plots, but also to test other possible redshift dependence of the SNe Ia rate (Kobayashi et al. 1998). The SNe Ia rate also depends on the assumed cosmological parameters. The cosmological parameters Ω_0 and λ_0 are now determined with $\sim 10\%$ accuracy in the combined analysis of Cosmic Microwave Background (CMB) experiments, SNe Ia, and large scale structure surveys (e.g., Sievers et al. 2002), and we assume the Ω_0 uncertainty to be $\Omega_0 = 0.3 \pm 0.05$ in the flat universe ($\Omega_0 + \lambda_0 = 1$). We also plot the resulting numbers of lensed SNe Ia for the constant R_{SN} model due to the Ω_0 uncertainty. We find that this level of uncertainty in Ω_0 does not significantly change the expected number of SNe so that we could still distinguish between models of the star formation history.

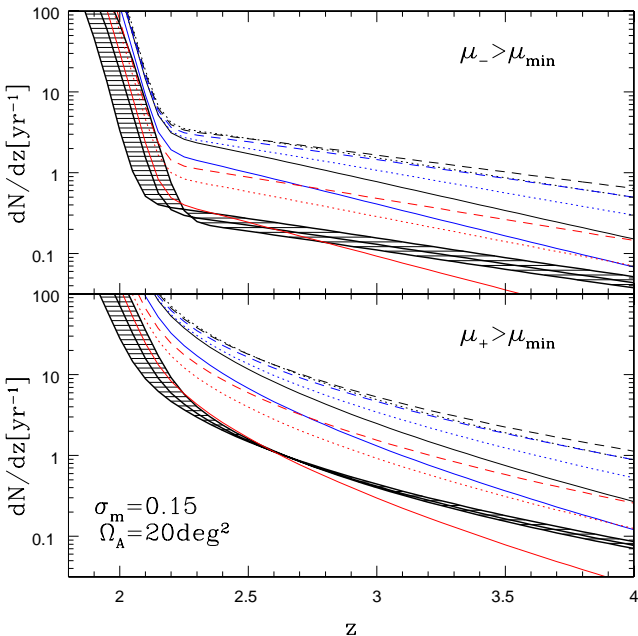


FIG. 2.— Numbers of lensed SNe Ia whose unlensed apparent magnitudes are fainter than the magnitude limit $m_{\text{lim}} = 30$ for the observed region of $\Omega_A = 20 \text{ deg}^2$. Lines are same as in Figure 1. For the constant R_{SN} model, we show the effect of different cosmological parameters ($\Omega_0 = 0.3 \pm 0.05$, $\Omega_0 + \lambda_0 = 1$) by the same three lines and shadings. We also impose a requirement that the photometry must extend 3.8 magnitudes below peak brightness (thus effectively $m_{\text{lim}} = 26.2$), and K-corrections are neglected. The limiting peak magnitude $m_{\text{lim}} = 26.2$ roughly corresponds to $z \sim 1.7$. The scatter of peak magnitude, $\sigma_m = 0.15$, is taken into account. A lambda-dominated universe is again assumed.

If both images are observed, we can infer the intrinsic magnitude of SNe Ia. For example, from the ratio of luminosities,

$$r = \frac{\mu_+}{\mu_-}, \quad (19)$$

the magnification factors become

$$\mu_+ = \frac{2r}{r-1}, \quad (20)$$

$$\mu_- = \frac{2}{r-1}. \quad (21)$$

The magnification factors also can be derived from the image separation and differential time delay if the redshift of the lens object is measured (see eq. [30]). The reconstruction of magnification factors could be used, in principle, to derive the distance-redshift relation at high- z and to estimate the cosmological parameters more robustly.

4. TIME DELAY BIAS

Since there is a time delay between multiple images, strong lensing statistics of transient phenomena such as SNe inevitably involve some missing events due to the finite duration of the survey observations. Therefore, in strong lensing statistics of SNe we should take account of this “time delay bias”, especially for large image separations.

For the joint probability distributions, the time delay bias is included as follows

$$P^{\text{TB}}(\Delta t, \theta; z_S) = P(\Delta t, \theta; z_S) f(\Delta t), \quad (22)$$

$$P^{\text{TB}}(> \Delta t, \theta; z_S) = \int_{\Delta t}^{\infty} P(\Delta t', \theta; z_S) f(\Delta t') d(\Delta t'), \quad (23)$$

where $f(\Delta t)$ is the fraction of lenses with time delays Δt that can be observed (the superscript TB explicitly indicates the Time-delay Bias). The image separation distribution then becomes

$$P^{\text{TB}}(\theta; z_S) = \int_0^{\infty} P(\Delta t', \theta; z_S) f(\Delta t') d(\Delta t'). \quad (24)$$

Then the corresponding *conditional* probability distributions are computed as

$$P^{\text{TB}}(\Delta t | \theta; z_S) = \frac{P^{\text{TB}}(\Delta t, \theta; z_S)}{P^{\text{TB}}(\theta; z_S)}, \quad (25)$$

using $P^{\text{TB}}(\theta; z_S)$ instead of $P(\theta; z_S)$ which does not take account of the time-delay bias (eq.[11]).

If the observational monitoring is carried out continuously for a period of t_{obs} , for instance, $f(\Delta t)$ is given by

$$f(\Delta t) = \begin{cases} 1 - \frac{\Delta t}{t_{\text{obs}}} & (\Delta t < t_{\text{obs}}), \\ 0 & (\Delta t > t_{\text{obs}}). \end{cases} \quad (26)$$

Then $P^{\text{TB}}(\theta; z_S)$ reduces to

$$\begin{aligned} P^{\text{TB}}(\theta; z_S) &= \left[1 - \frac{1}{t_{\text{obs}}} \int_0^{t_{\text{obs}}} P(> \Delta t | \theta; z_S) d(\Delta t) \right] P(\theta; z_S) \\ &\equiv T(\theta, z_S) P(\theta; z_S). \end{aligned} \quad (27)$$

This means that the time delay bias for the image separation probability distribution is simply expressed by the multiplication factor $T(\theta, z_S)$.

Probability distributions of strong gravitational lensing including time delay bias (eq. [27]) are shown in Figure 3,

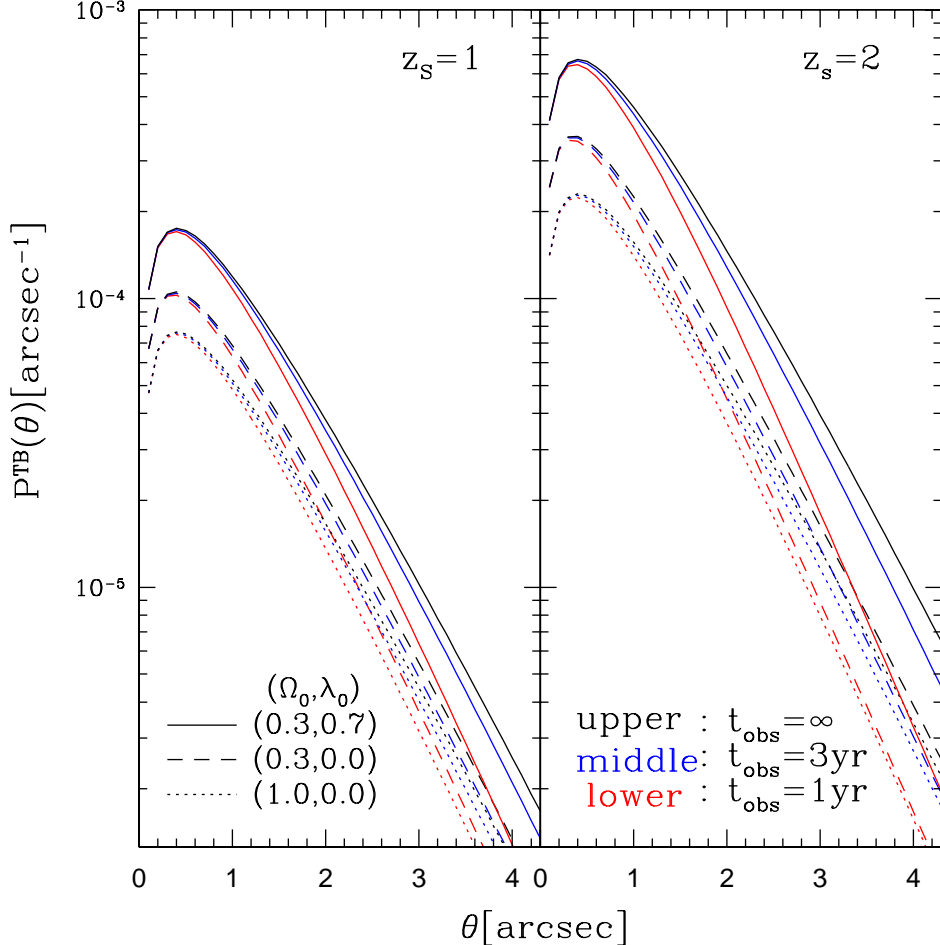


FIG. 3.— Probability distributions of strong gravitational lensing. The redshift of SNe is fixed to $z_s = 1$ (left) or 2 (right). The time delay bias (§4) is included, and continuous observations of $t_{\text{obs}} = \infty, 3\text{yr}$, and 1yr are considered. These probabilities are plotted for the three cosmological models with $h = 0.7$; $(\Omega_0, \lambda_0) = (0.3, 0.7)$, $(0.3, 0.0)$, and $(1.0, 0.0)$, in solid, dashed and dotted lines, respectively.

where we consider three cosmological models with $h = 0.7$; $(\Omega_0, \lambda_0) = (0.3, 0.7)$, $(0.3, 0.0)$, and $(1.0, 0.0)$. These probability distributions have been used to constrain cosmological constant (Turner 1990; Fukugita et al. 1992; Kochanek 1996; Chiba & Yoshii 1999), and are indeed useful as an independent measurement of cosmological parameters in the case of SNe survey (Wang 2000; Holz 2001; Goobar et al. 2002). These plots show that the time delay bias is more important for larger θ , because the time delay Δt is larger on average as θ increases. The amount of the time delay bias is, however, quite small for lensing of typical an image separation of $\theta \sim 1''$, if the observation time is larger than 1 year. For larger separation lensing, $\theta \sim 3''$, the time delay bias changes lensing probabilities by a factor 2 and thus is important in quantitative discussions.

Since the time delay bias is more important for larger separation lensing, we also calculate probability distributions for wide separation lensing in the lambda-dominated Cold Dark Matter (CDM) model, assuming a fluctuation amplitude $\sigma_8 = 1$ for simplicity. Although the expected wide separation lensing rate due to CDM halos is much smaller than for galaxy lensing, we still expect that wide separation lensing will be observed because core-collapse SNe as well as SNe Ia can be used for lensing statistics, which greatly increases the number of SNe (e.g., Goobar et al. 2002). Wide separation lensing is expected to reflect the properties of dark halos rather than (the visible parts

of) galaxies, thus it has been used to constrain the abundance of dark halos (Kochanek 1995) and density profile of dark halos (Maoz et al. 1997; Wyithe, Turner, & Spergel 2001; Keeton & Madau 2001; Takahashi & Chiba 2001; Li & Ostriker 2002; Oguri et al. 2002). We adopt the generalized form (Zhao 1996; Jing & Suto 2000) of the density profile proposed by Navarro, Frenk, & White (1997, hereafter NFW):

$$\rho(r) = \frac{\rho_{\text{crit}} \delta_c}{(r/r_s)^\alpha (1+r/r_s)^{3-\alpha}}, \quad (28)$$

where $r_s = r_{\text{vir}}/c_{\text{vir}}$ and c_{vir} is the concentration parameter. We adopt the mass and redshift dependence reported by Bullock et al. (2001) for $\alpha = 1$, and generalize it to $\alpha \neq 1$ by the multiplicative factor $(2-\alpha)$ (Keeton & Madau 2001). We also take account of scatter of the concentration parameter which has a log-normal distribution with a dispersion of $\sigma_c = 0.18$ (Jing 2000; Bullock et al. 2001). The characteristic density δ_c can be computed using the spherical collapse model (see Oguri, Taruya, & Suto 2001). As the mass function of dark halos, we adopt the fitting form derived by Sheth & Tormen (1999). From these, we predict probability distributions of wide separation lensing taking account of the time delay bias (see Oguri et al. 2002 for the calculation of time delay probability distributions in the case of generalized NFW density profile), and results are shown in Figure 4. Here we focus on large separation lensing ($\theta > 5''$) because the relation between small and large separation lensing

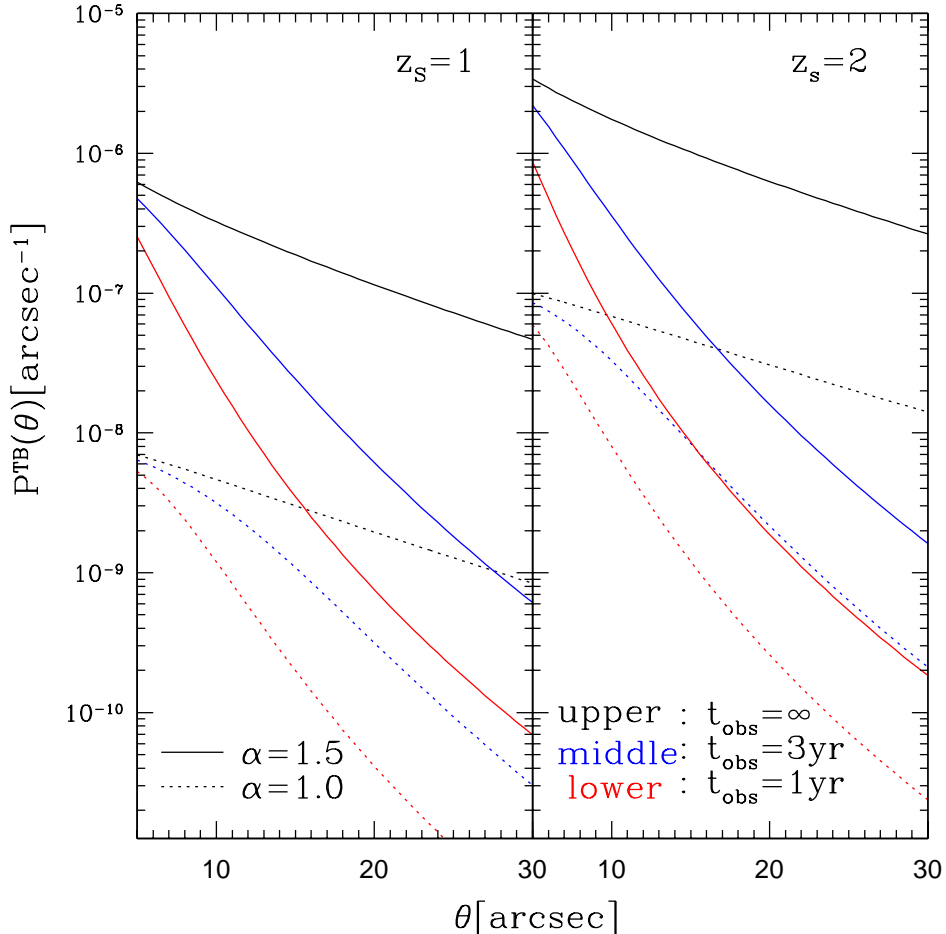


FIG. 4.— Probability distributions of strong lensing at wide separation, calculated by assuming the generalized NFW density profile (eq. [28]) and Sheth & Tormen (1999) mass function. We adopt the cold dark matter model in a lambda-dominated universe with the mass fluctuation amplitude $\sigma_8 = 1$. The time delay bias (§4) is included.

depends strongly on the model of galaxy formation and is difficult to determine unambiguously (Oguri 2002). This plot indicates that time delay bias is quite significant; it can suppress the lensing probability by one or two orders of magnitude. It is also found that the suppression due to time delay bias is larger for $\alpha = 1.5$ than $\alpha = 1.0$ because for a fixed separation θ , the time delays in the case of $\alpha = 1.5$ are on average larger than those in the case of $\alpha = 1.0$ (Oguri et al. 2002). This slightly compensates for the difference of lensing probabilities between various values of α , but the difference is still large (about one order of magnitude between $\alpha = 1.5$ and $\alpha = 1.0$). Therefore we conclude that statistics of wide separation SNe lensing still could provide a useful probe of density profile.

We also show the effect of the time delay bias on the time delay probability distribution in Figure 5. As seen in the figure, the time delay probability distributions for large θ are strongly affected by the finite duration of observations.

5. PREDICTIONS FOR TIME-DELAYED (TRAILING) IMAGES

Since the primary purpose of the proposed SNe Ia surveys is to construct the Hubble diagram, one may always assume that the source redshift of each SNe Ia, z_s , is determined spectroscopically. We are interested in unusually bright SNe Ia in the diagram. If the lensing object is approximated by an SIS, there are two images, x_{\pm} , and the brighter image (x_+) arrives first. Thus the difference between the observed magnitude of

those outliers (with respect the typical magnitude of the SNe Ia) and the average magnitude at the redshift can be ascribed to the lensing magnification μ_+ . While the standard deviation of the SNe Ia peak magnitude corrected for the lightcurve shape method is typically 0.15mag (Porciani & Madau 2000), multiple lensing images are produced if $\mu_+ \geq 2$ or equivalently more than 0.75mag. Thus 5σ outliers are strong candidates for multiple image lensed SNe Ia.

The lensing object (most likely an early-type galaxy) for those candidates is typically half way out in affine or angular diameter distance. For instance, an L^* galaxy at $z = 0.5$ is about 24th magnitude in the B-band, and the surface number density at this magnitude limit is ~ 30 per arcmin² or so. Since the typical image separation θ_+ is $1''$, the average number of galaxies within that angular separation from each lensed SNe Ia is much less than 1. Therefore it should be relatively easy to find candidates for the lensing galaxy and thus determine θ_+ , and even possibly the redshift of the candidate galaxy z_L .

Our next goal is to predict the location of the second image θ_- , and the time delay Δt by which the second image trails the first and brighter one. We consider the following three cases: (1) the magnification factor μ_+ , the redshift of the lens object z_L , and the angular separation from the lens object $\theta_+ = \xi_0 x_+ / D_{OL}$ are all known; (2) only μ_+ and θ_+ are known; (3) just μ_+ is known. In doing so, we have to assume a specific model for the lensing potential. We mainly show results for the SIS lensing

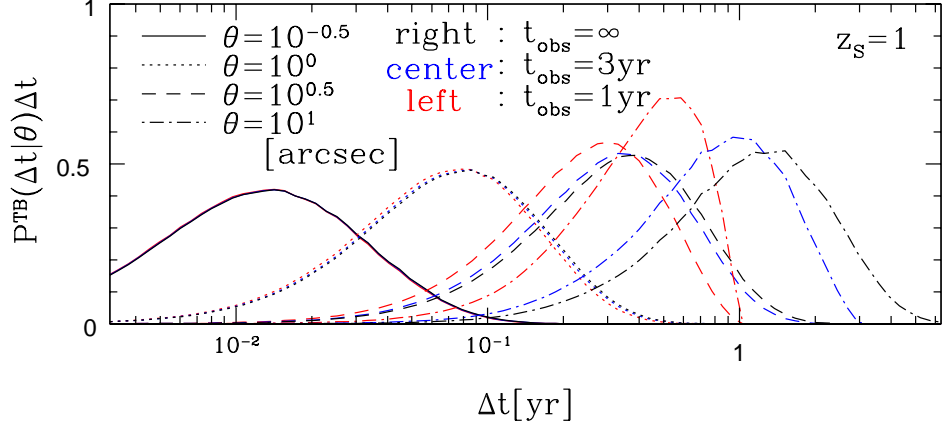


FIG. 5.— Conditional probability distributions of differential time delays. The time delay bias (§4) is included (as in Fig. 3). A lambda-dominated universe is assumed.

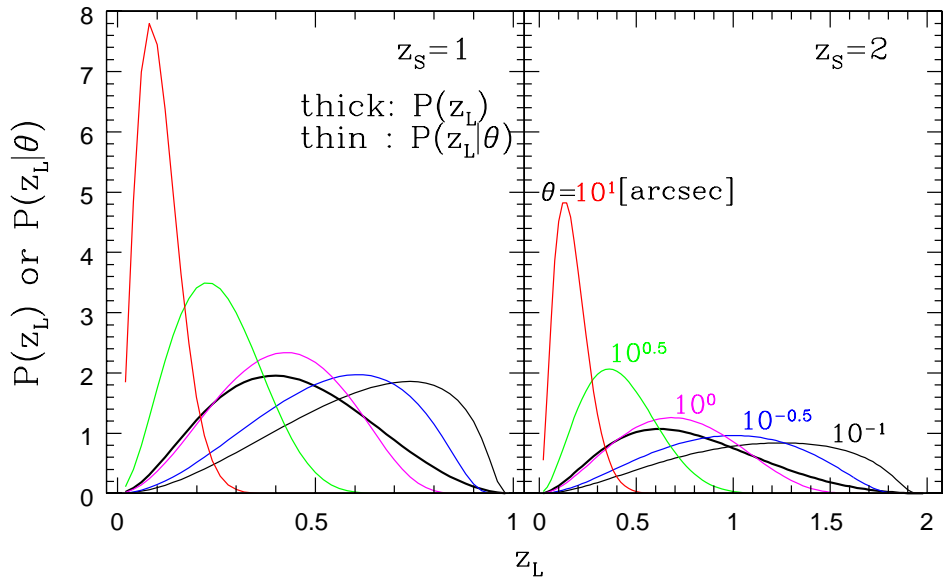


FIG. 6.— Distributions of lens redshift z_L (eqs. [32] and [38]). Thick lines are probability distributions of z_L when θ is unrestricted, $P(z_L)$ (eq. [32]) while thin lines are those when θ is fixed, $P(z_L|\theta)$ (eq. [38]). A lambda-dominated universe is assumed.

model (eq. [6]) but also present a comparison with the NFW halo model (eq. [28]).

5.1. Case 1: μ_+ , θ_+ , and z_L are known

We can obtain these three quantities when the lens candidate is identified and the redshift of that lens candidate is known. In this case, both the separation θ and the time delay Δt are uniquely determined as

$$\theta = 2\theta_+ \frac{\mu_+ - 1}{\mu_+}, \quad (29)$$

and

$$\Delta t = \frac{1}{2c} \frac{D_{OL} D_{OS}}{D_{LS}} (1+z_L) \theta^2 \frac{1}{\mu_+ - 1}. \quad (30)$$

We now consider errors induced by observable quantities. We assume that the redshifts are measured spectroscopically, thus errors from redshifts are negligible. As for the image separation θ_+ , SNAP would have an angular resolution of $0.1''$, which is also sufficient to determine θ_+ accurately for most purposes. The most important source of uncertainty is therefore μ_+ , because the magnification estimates may be inaccurate due

to substructure in the lens galaxies (Mao & Schneider 1998), dust extinction and/or the intrinsic spread in corrected SNe Ia peak luminosities, photometry, K-corrections and so forth. If μ_+ is sufficiently larger than 1 (this is correct for most strong lensing cases), we obtain $\Delta t \propto (\mu_+)^{-1}$ from equations (29) and (30). This means that errors in μ_+ directly affect Δt ; e.g., a 20% error in μ_+ results in a 20% uncertainty in the Δt estimation.

5.2. Case 2: μ_+ and θ_+ are known

This is the case in which there is a lens candidate but the redshift is not known (yet). We can predict the image separation from equation (29), but the time delay is ambiguous due to z_L , and has some probability distribution which reflects the distribution of z_L . We rewrite equation (30) as

$$\frac{\Delta t(\mu_+ - 1)}{\theta^2} = \frac{1}{2c} \frac{D_{OL} D_{OS}}{D_{LS}} (1+z_L) \equiv F. \quad (31)$$

Therefore we can obtain the probability distribution for the combination of $\Delta t(\mu_+ - 1)$, instead of Δt alone. To derive this, we should calculate the conditional probability distribution of z_L for fixed θ :

$$P(z_L|\theta; z_s) = \frac{P(z_L, \theta; z_s)}{P(\theta; z_s)}, \quad (32)$$

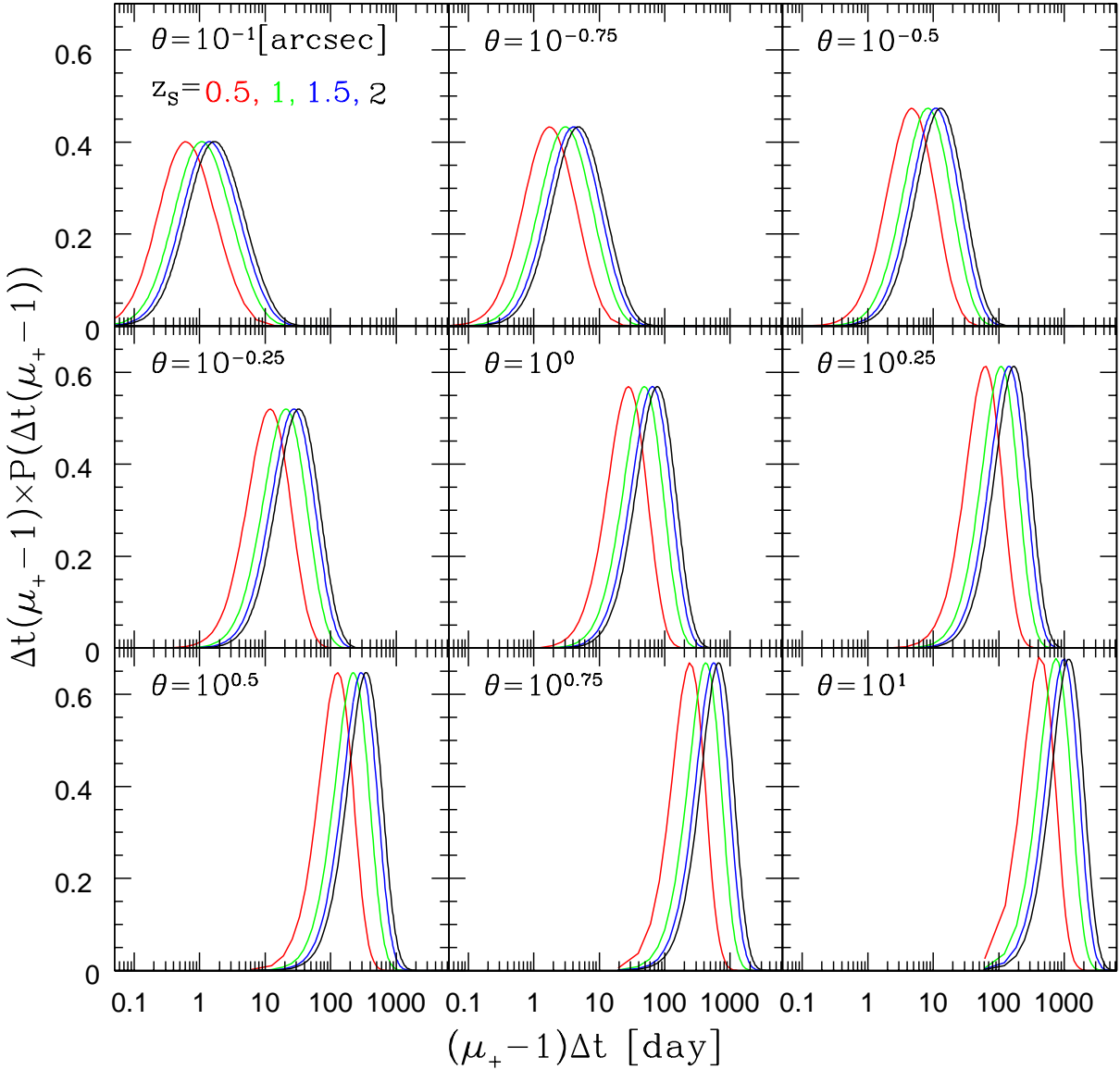


FIG. 7.—Predictions for the trailing image in “Case 2” (§5.2). Probability distributions of $(\mu_+ - 1)\Delta t$ (eq. [34] times $(\mu_+ - 1)\Delta t$) are plotted for various z_s and θ . A lambda-dominated universe is assumed.

where

$$P(z_L, \theta; z_s) = \left[\frac{dv}{d\theta} \frac{d\phi}{dv} \frac{cdt}{dz_L} (1+z_L)^3 \sigma_{\text{SIS}} \right]_{v=v_{\min}}. \quad (33)$$

We plot $P(z_L | \theta; z_s)$ for various θ values IN Figure 6. Then the distribution of $\Delta t(\mu_+ - 1)$ is

$$P(\Delta t(\mu_+ - 1)) = P(z_L | \theta; z_s) \left(\frac{dF}{dz_L} \right)^{-1} \frac{1}{\theta^2}. \quad (34)$$

The results are shown in Figure 7. These results are of course affected by observational uncertainties of μ_+ as mentioned in §5.1. If μ_+ is sufficiently large, errors in μ_+ do not affect θ since $\theta \sim 2\theta_+$ (see eq. [29]). On the other hand, Δt is directly affected by μ_+ because we obtain the probability distribution for $\Delta t(\mu_+ - 1)$. The width of this probability distribution is, however, about one order of magnitude, while errors induced by μ_+ are probably only a factor of 2 or so (Metcalf & Madau 2001; Chiba 2002; Dalal & Kochanek 2002). Therefore errors in μ_+ are not so serious as in the previous case.

In practice, we find a fitting formula of $P(\Delta t(\mu_+ - 1))$:

$$P(\Delta t(\mu_+ - 1))d(\Delta t(\mu_+ - 1)) = \frac{1}{\sqrt{2\pi}\sigma} \exp \left[-\frac{\{\ln(\Delta t(\mu_+ - 1)) - \ln a\}^2}{2\sigma^2} \right] d\ln(\Delta t(\mu_+ - 1)) \quad (35)$$

$$a = 4.28(-110 + 158z_s^{0.212})\theta^{1.63}(3.68 + \theta)^{-0.952} [\text{day}], \quad (36)$$

$$\sigma = 0.693 - 0.115(\ln\theta) + 0.0211(\ln\theta)^2 + 0.00347(\ln\theta)^3 - 0.00106(\ln\theta)^4, \quad (37)$$

where θ is in units of arcsec. This formula is valid for $0.5 \lesssim z_s \lesssim 4.0$ and $0.1'' \lesssim \theta \lesssim 10''$ which cover the range of our typical interest. The accuracy is $\lesssim 10\%$ around the peak (within $\sim 1.5\sigma$).

5.3. Case 3: μ_+ is known

This is the case in which a candidate for the lensing object is not identified. The distribution of z_L for an unrestricted θ is

$$P(z_L; z_s) = \frac{1}{P(z_s)} \int_0^\infty dv \frac{d\phi}{dv} \frac{cdt}{dz_L} (1+z_L)^3 \sigma_{\text{SIS}}, \quad (38)$$

where we normalize by the total probability of strong gravitational lensing:

$$P(z_S) = \int_0^{z_S} dz_L P(z_L; z_S). \quad (39)$$

From this distribution of z_S , we can calculate the probability distribution for $\Delta t(\mu_+ - 1)/\theta^2$:

$$P(\Delta t(\mu_+ - 1)/\theta^2) = P(z_L; z_S) \left(\frac{dF}{dz_L} \right)^{-1}. \quad (40)$$

Therefore we can predict the probability distribution for a combination of the time delay, the magnification and the image separation. Figure 8 plots this probability distribution for various z_S . Errors in μ_+ are not important for the same reason described in §5.2.

Again we find a fitting formula for $P(\Delta t(\mu_+ - 1)/\theta^2)$:

$$\begin{aligned} & P(\Delta t(\mu_+ - 1)/\theta^2) d(\Delta t(\mu_+ - 1)/\theta^2) \\ &= \frac{1}{\sqrt{2\pi}\sigma} \exp \left[-\frac{\{\ln(\Delta t(\mu_+ - 1)/\theta^2) - \ln a\}^2}{2\sigma^2} \right] \\ & \quad \times d\ln(\Delta t(\mu_+ - 1)/\theta^2), \end{aligned} \quad (41)$$

$$a = -110 + 158z_S^{0.212} \text{ [day]}, \quad (42)$$

$$\sigma = 0.846. \quad (43)$$

This formula is valid for $0.5 \lesssim z_S \lesssim 4.0$, and the accuracy is $\lesssim 10\%$ around the peak (within $\sim 1.5\sigma$).

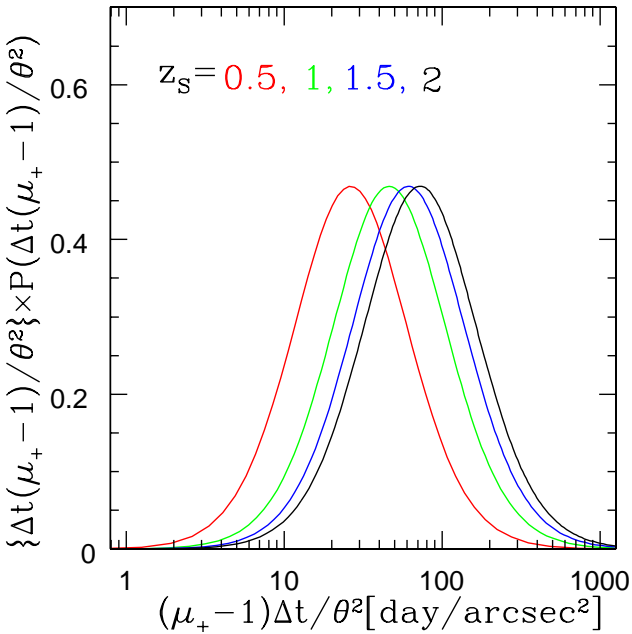


FIG. 8.— Predictions for the trailing image in “Case 3” (§5.3). Probability distributions of $(\mu_+ - 1)\Delta t/\theta^2$ (eq. [40] times $(\mu_+ - 1)\Delta t/\theta^2$) are plotted for various z_S . A lambda-dominated universe is assumed.

5.4. Case 2 & NFW profile

In this subsection, we consider a case in which the density profile of the lensing objects is well described by the generalized NFW profile (eq. [28]) instead of by a SIS. We retain the velocity function of galaxies (eq. [12]) previously used, since

we mainly want to elucidate the effect of different density profiles. In this case, differential time delays and image separations are approximated as (Oguri et al. 2002)

$$\Delta t = \frac{2r_s^2 x_t D_{\text{OS}}}{c D_{\text{OL}} D_{\text{LS}}} (1 + z_L) y, \quad (44)$$

$$\theta = \frac{2r_s x_t}{D_{\text{OL}}}, \quad (45)$$

where x_t is a radius of the tangential critical curve normalized by $\xi_0 = r_s$. We also assume that μ_+ is approximately given as

$$\mu_+ = \frac{\mu_{10} y_r}{2 y}, \quad (46)$$

where y_r is the radius of the radial caustic. The explicit form of μ_{10} may be found in Oguri et al. (2002). From these,

$$\mu_+ \Delta t = \theta^2 \frac{y_r \mu_{10}}{4 c x_t} \frac{D_{\text{OS}} D_{\text{OL}}}{D_{\text{LS}}} (1 + z_L), \quad (47)$$

and thus we can derive the probability distribution of $\mu_+ \Delta t$. Figure 9 shows the probability distribution of $\mu_+ \Delta t$ for inner slopes $\alpha = 0.5, 1.0$ and 1.5 in dashed, dotted and thin solid curves, respectively. This figure indicates that a smaller α predicts larger values of $\mu_+ \Delta t$. The dependence of Δt alone on α has the opposite sign; a steeper inner slope of the density profile have larger time delays on average (Oguri et al. 2002). The reason is that a shallower density profile tends to produce larger μ_+ values and thus to cancel the dependence of Δt and μ_+ on α . The effect of varying the assumed lens density profile is thus significantly reduced by competing effects.

6. DISCUSSION

We have studied strong gravitational lensing of distant supernovae with particular attention to their magnification and time-delay statistics. Since supernovae are both “standard candles” at peak brightness and transient phenomena, unlike more conventional lensed sources such as quasars, they have some unique and relatively unfamiliar properties.

One such feature of supernova lensing is that we can determine the magnification factor directly from observations, not just the magnification ratios between different images. Since SNe Ia are known to be an excellent standard candle, unusually luminous supernovae are always strong candidates for strong lensing. We have shown that the location and the time delay of the trailing images of a lensed supernova with a given magnification factor can be predicted with useful accuracy. We have further considered several cases, depending on whether the lensing galaxy can be identified or not and whether its redshift is known or not. Such predictions will allow targeted observing programs to study exceptionally interesting phases of SN explosions and the determination of extremely accurate time delays. While we have mainly considered lenses with an SIS density profile, we find that our results are not qualitatively sensitive to variations in this density profile, and specifically, that generalized NFW profile lenses produce quite similar effects.

Due to the finite duration of the event, strongly lensed SNe will not always have multiple images observable simultaneously. In many cases, the second (usually fainter) image will appear after the first (brighter) image has faded away. This leads to an observational bias against the detection of multiple lensing images in any realistic SNe survey. We have calculated this time delay bias analytically, on the basis of time delay probability distributions derived by Oguri et al. (2002). We find that time delay bias significantly changes the expected number of lensed SNe, especially at wide separations. More specifically,

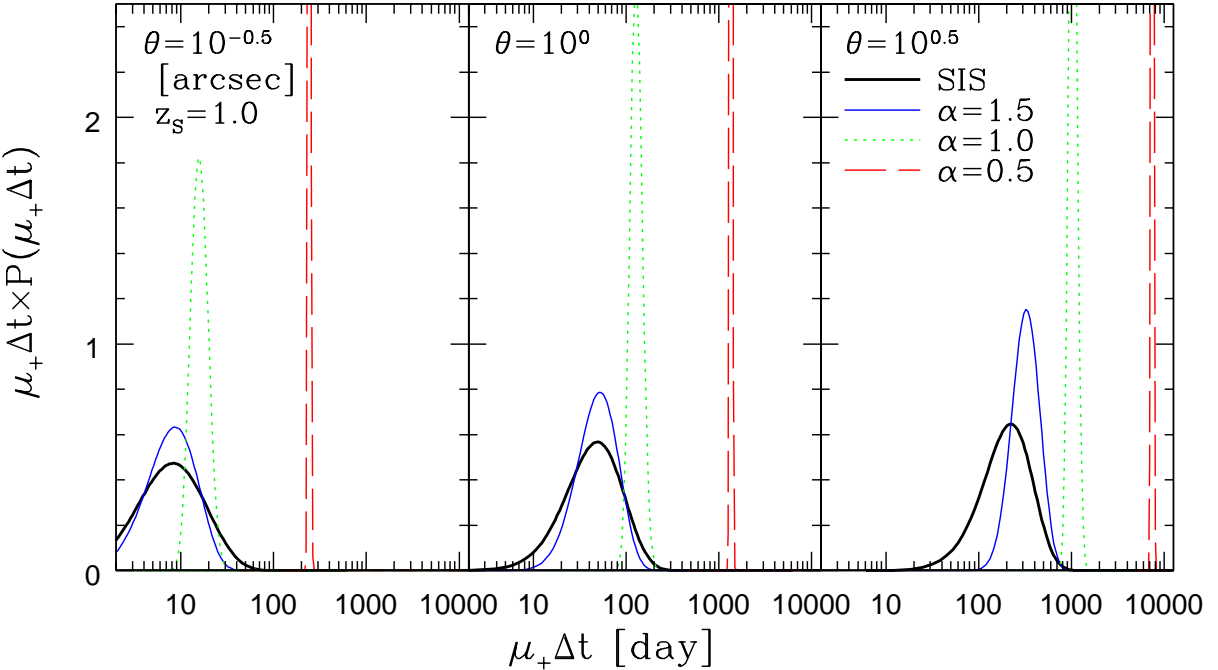


FIG. 9.—Predictions for the trailing image in “Case 2” using a generalized NFW density profile (eq. [28]). For the SIS case probability distributions of $(\mu_+ - 1)\Delta t$ instead of $\mu_+\Delta t$ are plotted. A lambda-dominated universe is assumed.

if the observational survey lasts of an order of a year, the lensing probability is suppressed by more than one order of magnitude at $\theta \sim 10''$. The suppression of the lensing probability is greater for a steeper inner density profile in the lensing objects. This is simply because a steeper inner profile yields a larger time delay (Oguri et al. 2002). We note that the time delay bias may have less effect on ground based SN surveys which are expected to operate for a longer term, such as LSST or a SN pencil beam survey like that proposed by Wang (2000).

In this paper we have studied spherically symmetric lenses. Although the inclusion of small ellipticities has little effect on the lensing cross section (Blandford & Kochanek 1987; Kochanek & Blandford 1987), it can yield lensing systems with four images. In such a more realistic case, our predictions for the time delays and image separations should correspond approximately to those for the pair of images with the largest separation in each quadrupole (their fractional errors are expected to be of order the ellipticity). Time delays among the other images can be much smaller than our predictions; e.g., the time delay between A1-A2 in PG1115+080 is expected to be much smaller (of order of one hour) than the time delay between B-C (~ 25 days) (e.g., Keeton & Kochanek 1997). The time delay bias for such systems might then be greatly reduced. In addition, four

images usually appear when the position of the source is close to that of the center of the lens galaxy. This will also cause four-images systems to have systematically smaller time delays. We thus expect that the ratio of four image to two image lens systems will be larger for lensed SNe than for other lens systems in which all images are continuously present.

Another pleasing aspect of strongly lensed SNe Ia is that they allow one to make a fairly straightforward *theoretical* prediction for a cosmologically distant phenomenon that is then subject to direct quantitative verification on a humanly practical time scale. This possibility is relatively rare in astronomy except in case involving intrinsically periodic phenomena, such as orbits or pulsar emission, where the “prediction” is basically empirical extrapolation rather than truly theoretical. It is particularly rare in a cosmological context. Although one certainly would not expect major surprises in comparing such predictions to future observations, it is still an important opportunity to test and validate our basic understanding of cosmology and gravitational theory.

This research was supported in part by the Grant-in-Aid for Scientific Research of JSPS (12640231, 14102004) and by NASA grant NAG5-9274.

REFERENCES

Bahcall, N. A., Ostriker, J. P., Perlmutter, S., & Steinhardt, P. J. 1999, *Science*, 284, 1481
 Blain, A. W., Kneib, J.-P., Ivison, R. J., & Smail, I. 1999, *ApJ*, 512, L87
 Blandford, R. D., & Kochanek, C. S. 1987, *ApJ*, 321, 658
 Bullock, J. S., Kolatt, T. S., Sigad, Y., Somerville, R. S., Kravtsov, A. V., Klypin, A. A., Primack, J. R., & Dekel, A. 2001, *MNRAS*, 321, 559
 Cappellaro, E., Evans, R., & Turatto, M. 1999, *A&A*, 351, 459
 Chiba, M. 2002, *ApJ*, 565, 17
 Chiba, M., & Yoshii, Y. 1999, *ApJ*, 510, 42
 Dalal, N., & Kochanek, C. S. 2002, *ApJ*, 572, 25
 Fukugita, M., Futamase, T., Kasai, M., & Turner, E. L. 1992, *ApJ*, 393, 3
 Gonzalez, A. H., Williams, K. A., Bullock, J. S., Kolatt, T. S., & Primack, J. R. 2000, *ApJ*, 528, 145
 Goobar, A., Mörtsell, E., Amanullah, R., & Nugent, P. 2002, *A&A*, 393, 25
 Hardin, D., et al. 2000, *A&A*, 362, 419
 Holz, D. E. 2001, *ApJ*, 556, L71
 Jing, Y. P. 2000, *ApJ*, 535, 30
 Jing, Y. P., & Suto, Y. 2000, *ApJ*, 529, L69
 Keeton, C. R., & Kochanek, C. S. 1997, *ApJ*, 487, 42
 Keeton, C. R., & Madau, P. 2001, *ApJ*, 549, L25
 Kobayashi, C., Tsujimoto, T., Nomoto, K., Hachisu, I., & Kato, M. 1998, *ApJ*, 503, L155
 Kochanek, C. S. 1995, *ApJ*, 453, 545
 Kochanek, C. S. 1996, *ApJ*, 466, 638
 Kochanek, C. S., & Blandford, R. D. 1987, *ApJ*, 321, 676
 Kolatt, T. S., & Bartelmann, M. 1998, *MNRAS*, 296, 763

Li, L. X., & Ostriker, J. P. 2002, *ApJ*, 566, 652

Madau, P., Della Valle, M., & Panagia, N. 1998 *MNRAS*, 297, L17

Madau, P., & Pozzetti, L. 2000, *MNRAS*, 312, L9

Mao, S., & Schneider, P. 1998, *MNRAS*, 295, 587

Maoz, D., Rix, H.-W., Gal-Yam, A., & Gould, A. 1997, *ApJ*, 486, 75

Metcalf, R. B., & Madau, P. 2001, *ApJ*, 563, 9

Navarro, J. F., Frenk, C. S., & White, S. D. M. 1997, *ApJ*, 490, 493

Oguri, M. 2002, *ApJ*, in press (astro-ph/0207520)

Oguri, M., Taruya, A., & Suto, Y. 2001, *ApJ*, 559, 572

Oguri, M., Taruya, A., Suto, Y., & Turner, E. L. 2002, *ApJ*, 568, 488

Ostriker, J. P., & Steinhardt, P. J. 1995, *Nature*, 377, 600

Pain, R., et al. 1996, *ApJ*, 473, 356

Pain, R., et al. 2002, *ApJ*, 577, 120

Perlmutter, S., et al. 1999, *ApJ*, 517, 565

Phillips, M. M. 1993, *ApJ*, 413, L105

Porciani, C., & Madau, P. 2000, *ApJ*, 532, 679

Porciani, C., & Madau, P. 2001, *ApJ*, 548, 522

Riess, A. G., et al. 1998, *AJ*, 116, 1009

Riess, A. G., Press, W. H., & Kirshner, R. P. 1996, *ApJ*, 473, 88

Sheth, R. K., & Tormen, G. 1999, *MNRAS*, 308, 119

Sievers, J. L., et al. 2002, *ApJ*, submitted (astro-ph/0205387)

Steidel, C. C., Adelberger, K. L., Giavalisco, M., Dickinson, M., & Pettini, M. 1999, *ApJ*, 519, 1

Sullivan, M., Ellis, R., Nugent, P., Smail, I., & Madau, P. 2000, *MNRAS*, 319, 549

Takahashi, R., & Chiba, T. 2001, *ApJ*, 563, 489

Turner, E. L. 1980, *ApJ*, 242, L135

Turner, E. L. 1990, *ApJ*, 365, L43

Turner, E. L., Ostriker, J. P., & Gott, J. R. 1984, *ApJ*, 284, 1

Wang, Y. 2000, *ApJ*, 531, 676

Wyithe, J. S. B., Turner, E. L., & Spergel, D. N. 2001, *ApJ*, 555, 504

Yungelson, L. R., & Livio, M. 2000, *ApJ*, 528, 108

Zhao, H. S. 1996, *MNRAS*, 278, 488